Published online 18 October 2016 *Nucleic Acids Research, 2016, Vol. 44, No. 21* **10491–10504**
doi: 10.1093/nar/gkw933

Structure of the 70S ribosome from human pathogen *Staphylococcus aureus*

Iskander Khusainov[1,2,†], Quentin Vicens[3,†], Anthony Bochler[3], François Grosse[3], Alexander Myasnikov[1], Jean-François Ménétret[1], Johana Chicher[3], Stefano Marzi[3], Pascale Romby[3], Gulnara Yusupova[1], Marat Yusupov[1,*] and Yaser Hashem[3,*]

[1]Département de Biologie et de Génomique Structurales, Institut de Génétique et de Biologie Moléculaire et Cellulaire, CNRS UMR7104, INSERM U964, Université de Strasbourg, Illkirch 67400, France, [2]Institute of Fundamental Medicine and Biology, Kazan Federal University, Kazan 420008, Russia and [3]Architecture et Réactivité de l'ARN, Université de Strasbourg, Institut de Biologie Moléculaire et Cellulaire du CNRS, Strasbourg 67084, France

Received August 26, 2016; Revised October 02, 2016; Editorial Decision October 06, 2016; Accepted October 06, 2016

ABSTRACT

Comparative structural studies of ribosomes from various organisms keep offering exciting insights on how species-specific or environment-related structural features of ribosomes may impact translation specificity and its regulation. Although the importance of such features may be less obvious within more closely related organisms, their existence could account for vital yet species-specific mechanisms of translation regulation that would involve stalling, cell survival and antibiotic resistance. Here, we present the first full 70S ribosome structure from *Staphylococcus aureus,* a Gram-positive pathogenic bacterium, solved by cryo-electron microscopy. Comparative analysis with other known bacterial ribosomes pinpoints several unique features specific to *S. aureus* around a conserved core, at both the protein and the RNA levels. Our work provides the structural basis for the many studies aiming at understanding translation regulation in *S. aureus* and for designing drugs against this often multi-resistant pathogen.

INTRODUCTION

Over the past decade, the stupendous developments in structural biology, including more recently in cryo-electron microscopy (cryo-EM; (1–3)), have extended our structural view of translation in profound ways. Ribosome structures from various species and cellular compartments have been solved, often in complex with multiple partners (see (4–10) for selected recent examples). These provide the basis for understanding how ribosomes vary in composition across species and cellular compartments, but also how they dynamically adjust to growth and stress conditions (11–14). Although we now have structural evidence for a common ribosomal core (15), species-specific features include paralogous ribosomal proteins (r-proteins) (16,17), functionally distinct ribosomal RNAs (rRNA) (18,19), differential rRNA or protein modifications (14) and rRNA expansion segments (20–22). Such variations may be found even within bacteria.

As an example of the structural adaptability of ribosomes, diverse bacterial species may carry different versions of the same r-protein, which may have evolved distinct functions as a result. For instance, bL25 contains one (as in *Escherichia coli*) or several domains (as in *Bacillus subtilis*), while a gene coding for bL25 is not present in many members of the *Bacilli* class (23). In *E. coli*, the N-terminal domain of bL25 binds to 5S rRNA to form part of the central protuberance (24–26). In *Thermus thermophilus*, the C-terminal domain of bL25 is involved in tRNA proofreading (27). Another characteristic r-protein is bS1, which in *E. coli* is essential for translation initiation of canonical mRNAs (28,29). bS1 comprises six OB-fold RNA binding domains in *E. coli*, but only four in *S. aureus* and other Gram-positive bacteria with low-GC content (30). Noteworthy, the N-terminal domain of bS1, which is missing in *S. aureus*, is responsible for binding to the small subunit (SSU) via bS2 in *E. coli* (28,31). Finally, a differential number of bL12 proteins (also called bL7 in its acetylated form) is bound to the ribosome according to the length of the 8th alpha helix of uL10. This interaction promotes the recruitment of various translation factors and stimulates GTP hydrolysis (32). Together, these examples illustrate how ribosome composition varies across bacteria, and how this may affect translation.

Ribosome composition may also be modulated in response to the environment. For example, the bS1 protein

*To whom correspondence should be addressed. Tel: +33 388 41 70 83; Fax: +33 388 60 22 18; Email: y.hashem@ibmc-cnrs.unistra.fr
Correspondence may also be addressed to Marat Yusupov. Tel: +33 388 65 33 01; Fax: +33 388 65 32 01; Email: marat@igbmc.fr
†These authors contributed equally to this work as the first authors.

is present in sub-stoichiometric amounts on 70S ribosomes under normal growth conditions, resulting in functional ribosome heterogeneity (33–35). Under specific stress conditions, subpopulations of ribosomes that do not contain bS1 accumulate to selectively translate leaderless mRNA (36,37). Some proteins like bL25 from *B. subtilis* are only expressed and bound to the ribosome under stress (38,39). Stress and various changes in growth conditions also lead to the stimulation of the acetylation of bL12/bL7 in *E. coli*, which increases the stability of the stalk complex through tightening the interaction between bL7 and uL10 (40). Another striking example of environmental modulation is illustrated by fluctuations in zinc concentration that trigger the expression of two paralogs of bL31 in *B. subtilis* (RpmE, referred to as A type and YtiA as B type). A and B types are distinguished by the presence of either Zn^{2+}-coordinating cysteines or a 15-amino-acid extension, respectively (12,41). The A type thereby serves as a storage mechanism for safely depositing loosely bound and potentially dangerous Zn^{2+} ions. The Zn^{2+}-dependent expression of the Zur transcription regulator represses the bL31_B gene, as well as those coding for components of the zinc-uptake systems, so that only the A type is expressed under normal conditions (42,43). When the zinc concentration becomes limiting, the B type is produced to replace the A type, due to its higher affinity for the ribosome (44). These various examples illustrate that bacteria employ different mechanisms (e.g. differential expression or chemical modification) in order to adjust to variations in their environment, which is suspected to impact translation. Additional regulation of translation or ribosome biogenesis could come from post-translational cleavage of r-proteins, as previously described for the firmicute-specific N-terminal extension of bL27 (45).

Ribosome tuning may also be achieved through alteration of the rRNA component based on environmental changes, as observed for some bacteria (37) and eukaryotes (18,19). In bacteria, both 16S and 23S rRNA contain insertions, which typically protrude from the ribosome to different extents. For example, h6, h10, h26 and h44 in the SSU, but also H28 and H68 in the large subunit (LSU) have different lengths or adopt different folds and orientations, as revealed when comparing the structures of 70S ribosomes from *E. coli*, *T. thermophilus* and *B. subtilis* (10,46–50) and the structure of the LSU from *Staphylococcus aureus* (51). Such variations in peripheral extensions suggests an involvement in translation regulation at one or several stages of the process.

Although whole-genome sequencing and sequence alignments have shown bacteria-specific differences in ribosomes, most structural studies that could highlight functional differences have been performed on Gram-negative organisms only, namely *T. thermophilus* and *E.coli* (52). Only recently two more ribosomal structures were solved at comparable resolutions from Gram-positive species, the full ribosome from *B. subtilis* and the large ribosomal subunit from *S. aureus*, by cryo-EM and X-ray crystallography, respectively (10,51,53). The lack of structural studies of additional bacterial species is one of the most important shortcomings in understanding vital and clinically relevant species-specific translation regulation mechanisms, including antibiotic resistance.

Considering how much remains to be discovered about ribosome diversity among bacteria and its impact on ribosome function, we solved at a resolution of 3.8 Å a cryo-EM structure of the 70S ribosome from human pathogen *S. aureus*. Our structure not only confirms the species-specific structural features identified previously in the LSU (51), but it reveals similarly variable features in the SSU, at both the rRNA and protein levels. The comparison of ribosomal structures from four different species of bacteria pinpoints variable regions in bacterial ribosomes, highlighting several species-specific features and suggesting their possible functional roles. Specifically, we discuss the fold of bL31 type B, which is the only bL31 paralog encoded by the *S. aureus* genome. On the rRNA side, we describe several rRNA insertions and particularities that might be involved in translation modulation. Most importantly, our work offers the fourth structure of a complete ribosome from any bacteria at near-atomic resolution, and the second of a Gram-positive bacterium. As *S. aureus* is an opportunistic pathogen that may cause significant skin, tissue and systemic infections (54–56), we anticipate that our structure will provide a solid basis for future studies of protein synthesis, and of its regulation for making virulence factors. Our work therefore represents an initial structural framework for developing effective strategies in order to combat infections.

MATERIALS AND METHODS

Bacterial growth and harvesting

In this study, we employed the RN6390 strain of *Staphylococcus aureus*, which derives from strain NCTC8325. This strain carries a deletion of the *rbsU* gene (normally coding for an activator of the σ^B factor), so that the transcription of RNAIII is strongly enhanced. As a result, this strain has a decreased ability to form biofilms (57).

Two liters of *S. aureus* culture were grown at 37°C (180 rpm) in Brain Heart Infusion broth and harvested in early logarithmic phase ($A_{600} = 1.0$ AU.ml^{-1}). Cells were washed twice with 10 mM Tris-HCl pH 7.5, pelleted at 4750 $\times g$, and the cell pellet was frozen at −80°C. A typical yield was 4.5–5.0 g of cells from 2 l of cell culture.

Ribosome purification

For 5 g of cells, the pellet was re-suspended in 30 ml of buffer A (20 mM HEPES-KOH pH 7.5, 100 mM NH_4Cl, 21 mM $Mg(OAc)_2$, 1 mM ethylenediaminetetraacetic acid (EDTA), 1 mM DTT), supplemented with the addition of 600 µl of protease inhibitor cocktail (one tablet (Roche), dissolved in 1 ml buffer A), of 300U DNase I (Roche) and of 3.5 mg lysostaphin (Sigma-Aldrich), before being lysed at 37°C for 45 min. Cell debris were removed by centrifugation at 30 000 $\times g$ for 90 min.

The resulting supernatant was further subjected to a differential precipitation by PEG, similarly to the protocol employed for *Saccharomyces cerevisiae* (58). PEG 20 000 was added from a 30% w/v stock solution (Hampton Research) to a final concentration of 2.8% w/v for the first fractionation. The solution was then centrifuged at 20 000 $\times g$ for 5 min. The supernatant was recovered and PEG 20 000 was

increased to 4.2% w/v for the second fractionation. The solution was then centrifuged at 20 000 $\times g$ for 10 min, and the ribosome pellet was resuspended in 35 ml buffer A and layered on 25 ml of a sucrose cushion (10 mM Hepes-KOH pH 7.5, 500 mM KCl, 25 mM $Mg(OAc)_2$, 1.1 M Sucrose, 0.5 mM EDTA, 1 mM DTT). Centrifugation was subsequently carried out at 45 000 rpm for 15 h using a Beckman Type 45 Ti rotor.

The crude ribosome pellet was resuspended in buffer E (10 mM Hepes-KOH pH 7.5, 100 mM KCl, 10 mM $Mg(OAc)_2$, 0.5 mM EDTA, 1 mM DTT) up to a concentration of 7 $mg.ml^{-1}$. Exactly 0.5 ml were loaded on 7–30% sucrose density gradients and centrifuged at 17 100 rpm for 15.5 h using a Beckman SW28 rotor. The fractions corresponding to 70S particles were pooled, the concentration of $Mg(OAc)_2$ was adjusted to 25 mM and PEG 20 000 was added to a final concentration of 4.5% w/v. Ribosomes were pelleted by centrifugation at 20 000 $\times g$ for 12 min, the pellet was gently dissolved in buffer G (5 mM Hepes-KOH pH 7.5, 50 mM KCl, 10 mM NH_4Cl, 10 mM $Mg(OAc)_2$, 1 mM DTT) to a final concentration of 20–25 $mg.ml^{-1}$. Aliquots of 30 μl were flash frozen in liquid nitrogen and stored at −80°C. A typical yield was 10–12 mg of ribosomes from 5 g of cells.

Analytical ultracentrifugation

Experiments were conducted at 4°C using a Beckman Coulter Proteome Lab XL-I analytical ultracentrifuge, with the 8-hole Beckman An-50Ti rotor. Ribosomes were thawed and diluted in buffer G to a concentration of 1.0 $A_{260}U.ml^{-1}$. The sample (400 μl) was loaded into one of the two quartz cuvettes of the centrifuge tube. The reference cuvette was filled with 410 μl of buffer G. Sedimentation at 20 644 $\times g$ was monitored by measuring the absorbance at 280 nm and 260 nm, with scans taken every 4 min. The density and viscosity of buffer G were calculated using the Sedntrep software. Data were analyzed using a c(s) model in SEDFIT (59).

Mass spectrometry

Mass spectrometry (MS) analysis was carried out at the IBMC proteomic platform, Strasbourg. The ribosome sample was analyzed by nano-LC-MS/MS on a NanoLC-2DPlus system (nanoFlexChiP module; Eksigent, ABSciex, Concord, Ontario, Canada) coupled to a TripleTOF 5600 mass spectrometer (ABSciex). The protein sample was precipitated, digested by trypsin and 500 ng of digested peptides were injected in the mass spectrometer. Protein identifications were assigned using the Mascot algorithm (version 2.2, Matrix Science, London, UK) through the ProteinScape 3.1 package (Bruker Daltonics, Leipzig, Germany). Searches were performed against the Swissprot database (January 2013 release), and the *S. aureus* taxonomy and identifications from Mascot were validated with a protein false discovery rate (FDR) < 1%.

Electron microscopy

Grid preparation. The purified 70S (4 μl at ∼ 0.150 $mg.ml^{-1}$ concentration (80 nM)) were applied to 400 mesh carbon-coated holey carbon Quantifoil 2/2 grids (Quantifoil Micro Tools, Jena, Germany; glow discharge time = 20 s), blotted with filter paper from both sides for 1.5 s in a temperature- and humidity-controlled Vitrobot apparatus Mark IV (FEI, Eindhoven, Netherlands, T = 4°C, humidity 100%, blot force 5, blot waiting time 30 s) and vitrified in liquid ethane pre-cooled by liquid nitrogen.

Image acquisition. Data were collected on the spherical aberration (Cs) corrected Titan Krios S-FEG instrument (FEI, Eindhoven, Netherlands) operating at 300 kV acceleration voltage and at a nominal underfocus of Δz = −0.6 to −4.5 μm using the second-generation back-thinned direct electron detector CMOS (Falcon II) 4096 × 4096 camera and automated data collection with EPU software (FEI, Eindhoven, Netherlands). The microscope was carefully aligned as well as the Cs corrector. The Falcon II camera was calibrated at a nominal magnification of 59 000 X. The calibrated magnification on the 14 μm pixel camera was 127 272 X, resulting in 1.1 Å pixel size at the specimen level. Camera was set up to collect 7 frames (start form the second one) out of 17 possible. Total exposure was 1 second with a dose of 60 $\bar{e}/Å^2$ (or 3.5 $\bar{e}/Å^2$ per frame). A total of 3850 images were collected.

Image processing. A framework for image processing employing several software packages (60) was used to obtain the 3D reconstruction of the *S. aureus* 70S.

Before particle picking, 7 frames in the stack were aligned using the Optical Flow algorithm integrated in Xmipp3 (61). Then, an average image of the whole stack was used to determine the contrast transfer function by CTFFIND4 (62) and to select semi automatically ∼423 500 particles in SCIPION (63). Particle sorting was done by 3D classification using RELION (64) leading to several 3D-classes (Supplementary Figure S1). Further classification was applied to two classes (Rotated P/E conf. 1 and conf. 2). At the end, 8 classes were derived in total from the entire data set, unrotated vacant 70S, unroated 70S with residual P and E tRNAs (probably due to the persistence of a fraction of tRNA in the 70S after washing) and 6 classes of rotated 70S ribosome presenting a P/E tRNA and all different in the degree of the 30S rotation.

All classes were refined using RELION's 3D autorefine and the final refined classes were then post-processed using the procedure implemented in RELION, which applies appropriate masking, B-factor sharpening and resolution validation to avoid over-fitting (64). The average resolution is ∼3.8 Å for the major class (unrotated, vacant, out of ∼110 000 particles). The resolution of the other classes (ranging from 4.7 to 7.3 Å) is indicated in Supplementary Figure S1. Determination of the local resolution of the final density map was performed using ResMap (65).

Map fitting and model refinement

The crystal structure of the LSU from *S. aureus* (PDB ID 4WCE; (51)) was fitted in the density map using Chimera v. 1.10.2 (66). RNA regions that were not seen in the X-ray crystal structure but were present in our density map were modeled using the cryo-EM structure from the 70S ribosome of *B. subtilis* (PDB ID 3J9W; (10)). Threading of the

23S rRNA was performed within Assemble v. 2 (67) (Supplementary Figure S2). The *B. subtilis* structure was also used as a template for modeling (using the Swiss-Model webserver (68)) the regions of proteins uL2, uL6, uL18, bL31 and bL32 that were not visible in 4WCE but were present in 3J9W and in our structure (Supplementary Figure S3). Protein secondary structures were also restored using Swiss-Model prior to map fitting (Supplementary Figure S3B and C). In the absence of any pre-existing structural model for the SSU, we used a similar approach to model the complete 16S rRNA, as well as 19 of the 21 SSU proteins that were visible in the density.

Molecular dynamics flexible fitting (MDFF; (69)) was performed for the complete 70S ribosome in VMD v. 1.9.2 (70), using NAMD v. 2 (gscale 0.3, numsteps 500 000, minsteps 2000) (71). The output .pdb file from MDFF was used as input for real-space refinement in Phenix v. 1.10.1-2155 (72,73). The refinement procedure included simulated annealing (starting temperature = 800 K) and global minimization for five macro-cycles, and took into account RNA and protein secondary structure restraints (search_method = from_ca). RNA geometry and fit in density were improved by running Erraser within Phenix (74,75), for rRNA fragments of ∼990 nt that overlapped by 2–4 nt. Model and map were inspected and adjusted in Coot v. 0.8.2 (76), using tools for real-space refinement, geometry regularization, morphing and backbone adjustments (Rcrane; (77)). In order to locate metal ion binding sites, we calculated a difference map in Chimera by subtracting a map we simulated at 4.0 Å using our metal-free model (CC = 0.88 Å) from the original density map. Partially or fully hydrated metal ions were placed according to stereochemistry and geometry in Coot (78,79). Final minimization of coordinates, including refinement of atomic displacement parameters, were carried out in Phenix v. dev-2341 (global minimization for 7–10 macro-cycles with hydrogen atoms, with secondary structure restraints (search_method = cablam) and restraints on metal ions that were not fully hydrated). For model validation, we used the Molprobity webserver (80) and model-to-map fit statistics from Phenix.

RESULTS

Determination of the cryo-EM structure of *S. aureus* ribosomes

70S ribosomes were isolated from *S. aureus* strain RN6390, whose ability to form biofilms is reduced (57). They were then purified according to a procedure similar to the ones we followed earlier to obtain bacterial 70S and eukaryotic 80S ribosomes suitable for structural analysis (48,58,81,82). In the case of *S. aureus* 70S ribosomes, we maximized both yield and quality of the sample through optimization of (i) the ionic conditions for lysis, (ii) the magnesium and PEG concentrations for ribosome precipitation and (iii) the sucrose concentration for setting up density gradients. After freezing and thawing, our preparations contained >90% of assembled, pure and homogenous 70S particles, as shown by denaturing gel analysis, analytical ultracentrifugation and the examination of cryo-electron micrographs (Figure 1A–C). Furthermore, we analyzed our preparation by mass spectrometry, which confirmed the presence of all r-proteins, except bS1, uS14 and bL9 (Supplementary Table S1). As we could identify uS14 but not the other two proteins in the structure, bS1 and bL9 may have been lost in the course of the purification procedure. Eight additional non-ribosomal proteins were also identified (Supplementary Table S1).

After data collection and processing (Table 1), eight conformationally variant 3D reconstructions were derived (Supplementary Figure S1), which mostly differ in the SSU degree of rotation and the conformations of the tRNA when it is present (mainly P/E tRNA). Only the major class was extensively analyzed, which corresponds to an unrotated 70S, mostly vacant (residual P-site tRNA can be observed), at an average resolution of 3.8 Å (Figure 1). As for the remaining seven classes, our analysis focused only on the relative rotation of the SSU compared to the major unrotated class (Supplementary Figure S1). No other noticeable structural variations were observed for these classes.

As typically observed for a ribosome cryo-EM reconstruction, the resolution of this 70S varies locally from ∼3.0 Å for the most stable regions, such as the core of the LSU, to ∼7.0 Å for the most flexible peripheral rRNA elements and some regions of the SSU head (Figure 1E). On average, the resolution of the LSU is also higher than that of the SSU (except for the L1 stalk), with the head of the SSU being the most flexible region. The refinement of atomic displacement parameters in real space further helps to visualize these ribosome dynamics (Supplementary Figure S4).

Overall, the three-dimensional structure of this vacant 70S ribosome from *S. aureus* contains >99% of all rRNA residues, 27 r-proteins in the LSU and 19 r-proteins in the SSU (Figure 2). No density was observed at the locations of bS1 and bL9 that further supports their absence first revealed by the MS analysis (Supplementary Table S1). Furthermore, the flexible r-proteins bS21, uL1, bL7/L12, uL10 and uL11 were excluded from our model, due to weak electron density that prevented us from modeling them with confidence (Supplementary Figure S5). Some proteins are only partially visible in the density maps, as for example bL25 and bL33 (Supplementary Table S2; Figure S6). At a resolution of 3.8 Å, we distinguish most nucleobases from backbone atoms within rRNA chains, and side-chains from backbone atoms within protein chains, especially when they contain rings (Figure 2F–I). We also located 32 metal ion binding sites, including a Zn-binding site in bL36 (no density for the metal ion is observed for other Zn-containing r-proteins such as bS2), and a divalent metal ion simultaneously coordinated to two purine N7 atoms (Figure 2J and K).

Structural differences between bacterial ribosomes cluster to regions facing the solvent

In order to pinpoint structural features that may be specific to the 70S ribosome from *S. aureus*, we compared its structure to that of the previously solved MifM-stalled 70S ribosome from *B. subtilis* (10), the only other structure available at medium-high resolution for a ribosome from Gram-positive bacteria. We also superimposed our structure with that of a vacant 70S ribosome from *E. coli* (47), and with

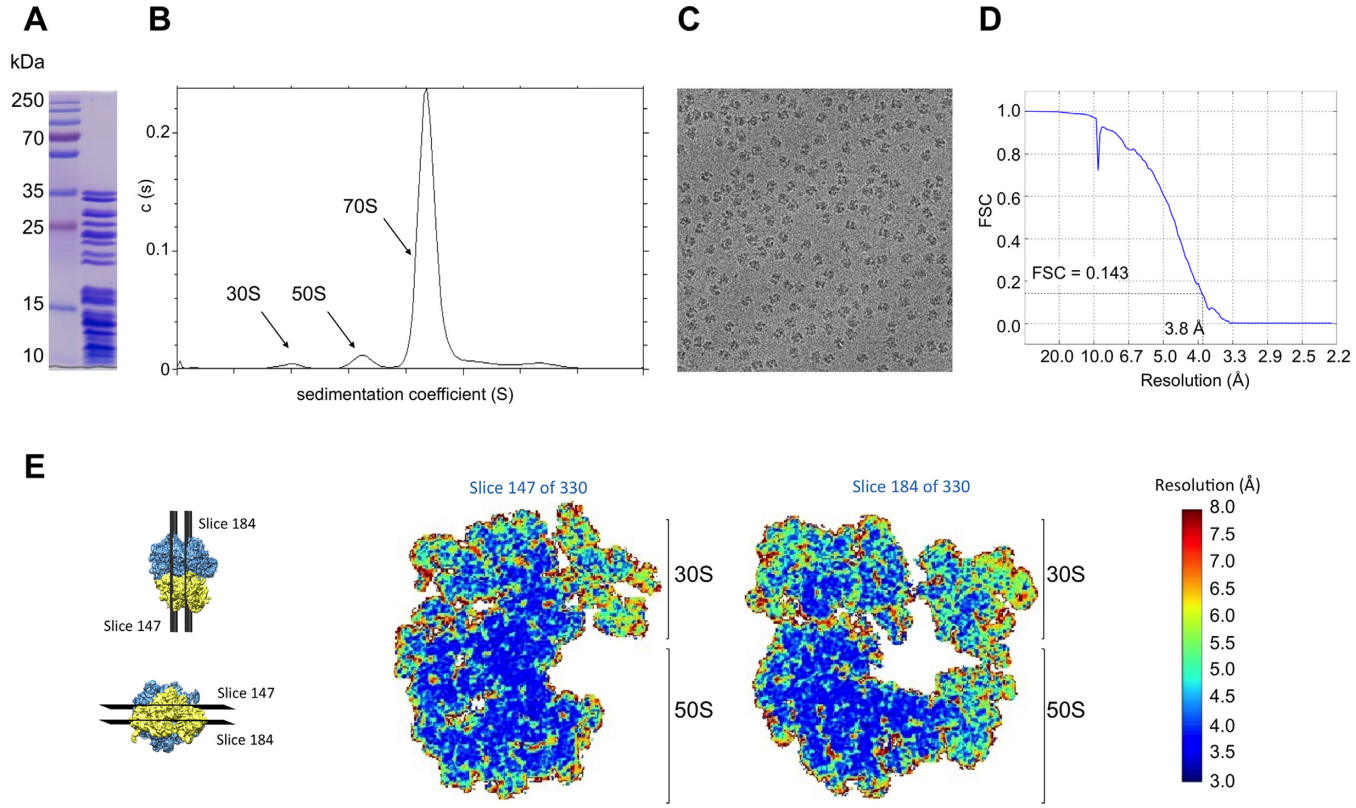

Figure 1. Sample characterization, cryo-EM data collection and processing. (**A**) SDS-PAGE of the *S. aureus* 70S sample demonstrating its purity. (**B**) Sedimentation profile showing the majority of material as stable 70S particles. (**C**) Representative electron micrograph showing the distribution of the 70S particles. (**D**) Fourier Shell Correlation (FSC) curve indicating the overall resolution of the *S. aureus* 70S ribosome structure. (**E**) Local resolution (rainbow scale) displayed on representative slices of the density map for the full ribosome.

that of a 70S-(A-P-E)tRNA-mRNA complex from *T. thermophilus* (83). In addition, we have compared the LSU in our structure to that recently solved by X-ray crystallography (51).

As reported earlier (10,51), bacterial ribosome structures are overall similar in their global structures. Also, the LSU in our structure solved by cryo-EM is similar to that solved by X-ray crystallography (all-atom RMSD = 3.1 Å; Supplementary Figure S7A and B) (51) regarding the commonly solved ribosomal regions (∼80%). The structural differences between r-proteins and rRNAs from the four species we surveyed are mostly located at the solvent-side of the two subunits (Figure 3; Supplementary Tables S2 and S3; Supplementary Figures S6 and S8). For r-proteins, differences are spread out over the surface of the ribosome. However, for rRNAs they remain on the body of the LSU, and the spur region of the SSU. Interestingly, h26 and h33 located at the exit and near the entry of the mRNA channel, respectively, appear to present the most important differences on the SSU compared to other species (Figure 3C and D). These peculiarities on both sides of the mRNA channel indicate possible roles for h26 and/or h33 in species-specific translation.

Examples of species-specific structural features

The structures of the 70S from *S. aureus* and from *B. subtilis* (10,51) confirm the subtleness of species-specific features among bacterial ribosomes. However, structural differences may have important functional and physiological consequences. Indeed, few unique structural differences in r-proteins and rRNAs suffice to distinguish bacteria according to species. If one disregards differences caused by the presence/absence of tRNAs or other factors in some of the surveyed structures (as in uL6, uL16, bL27), we notice unique species-specific extensions of uS9, uL3 and bL31 in *S. aureus*, of uS14 in *E. coli*, and of uS8, bL19 and bL28 in *T. thermophilus* (Supplementary Table S2; Supplementary Figure S6). Two loops (24–40 in uS12 and 67–80 in bL17) are present with a similar conformation in only Gram-positive bacteria (Supplementary Table S2; Supplementary Figure S6).

A remarkable example of ribosome variability is protein bL31. As described earlier (27), bL31 bridges the two subunits (Figure 4A), where it interacts with uS13, uS19 on the head of the SSU and with uL5 and the 5S rRNA on the central protuberance of the LSU. Our structure of the *S. aureus* 70S ribosome reveals the fold of a B-type paralog of bL31 (type A is not encoded in *S. aureus*), which comprises an extension of 15 amino acids in place of a zinc-binding motif (mostly Ser and Thr are found instead of the Zn^{2+}-coordinating Cys residues) (Figure 4). B-type bL31 folds similarly to A-type paralogs from other bacteria, and includes a three-stranded beta sheet near the N-terminus and a C-terminal extension, which may contain an alpha helix

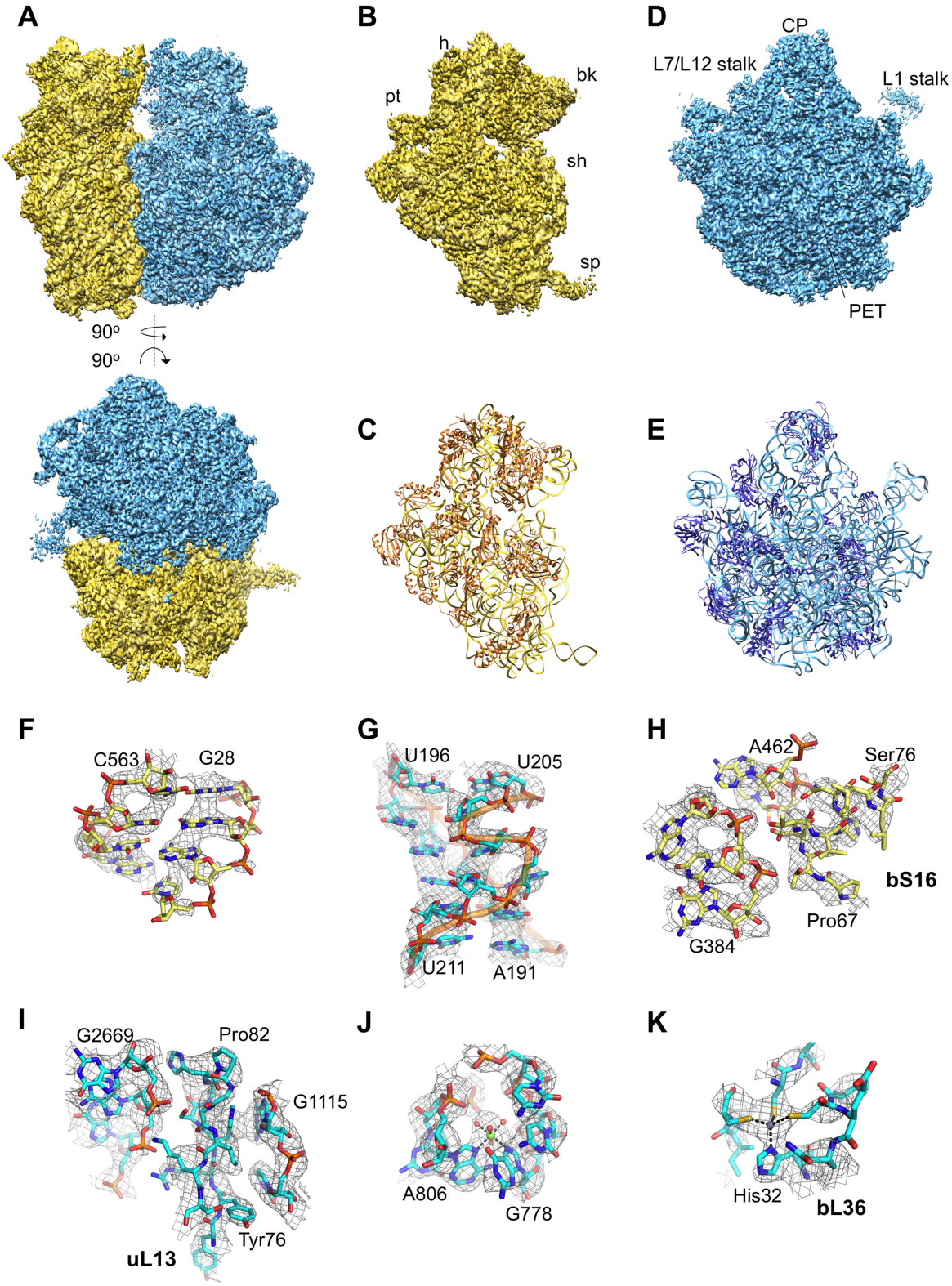

Figure 2. Structure of the *Staphylococcus aureus* ribosome. (**A**) Cryo-EM density map at 3.8 Å resolution (yellow, SSU; cyan, LSU), viewed from two different orientations. (**B**) Solvent side view of the SSU, indicating the main structural elements (h, head; bk, beak; pt, platform; sh, shoulder; sp, spur). (**C**) Cartoon view of the SSU model, oriented as in (B) (yellow, RNA; orange, proteins). (**D**) Solvent side view of the LSU, indicating the main structural elements (CP, central protuberance; PET, peptide exit tunnel). (**E**) Cartoon view of the LSU model, oriented as in (D) (cyan, RNA; blue, proteins). (**F**) A-form helix within the 16S rRNA (contour, 3.0 σ). (**G**) G-bulge motif located in the 23S rRNA (contour, 2.5 σ). (**H**) RNA-protein interface involving an α-helix from bS16 (contour, 2.5 σ). (**I**) RNA-protein interface involving a β-sheet from uL13 (contour, 2.5 σ). (**J**) Divalent metal ion binding site within the 23S rRNA (contour, 2.5 σ). (**K**) Zinc-binding site within protein bL36 (contour, 2.5 σ). Select residues are labeled in all panels.

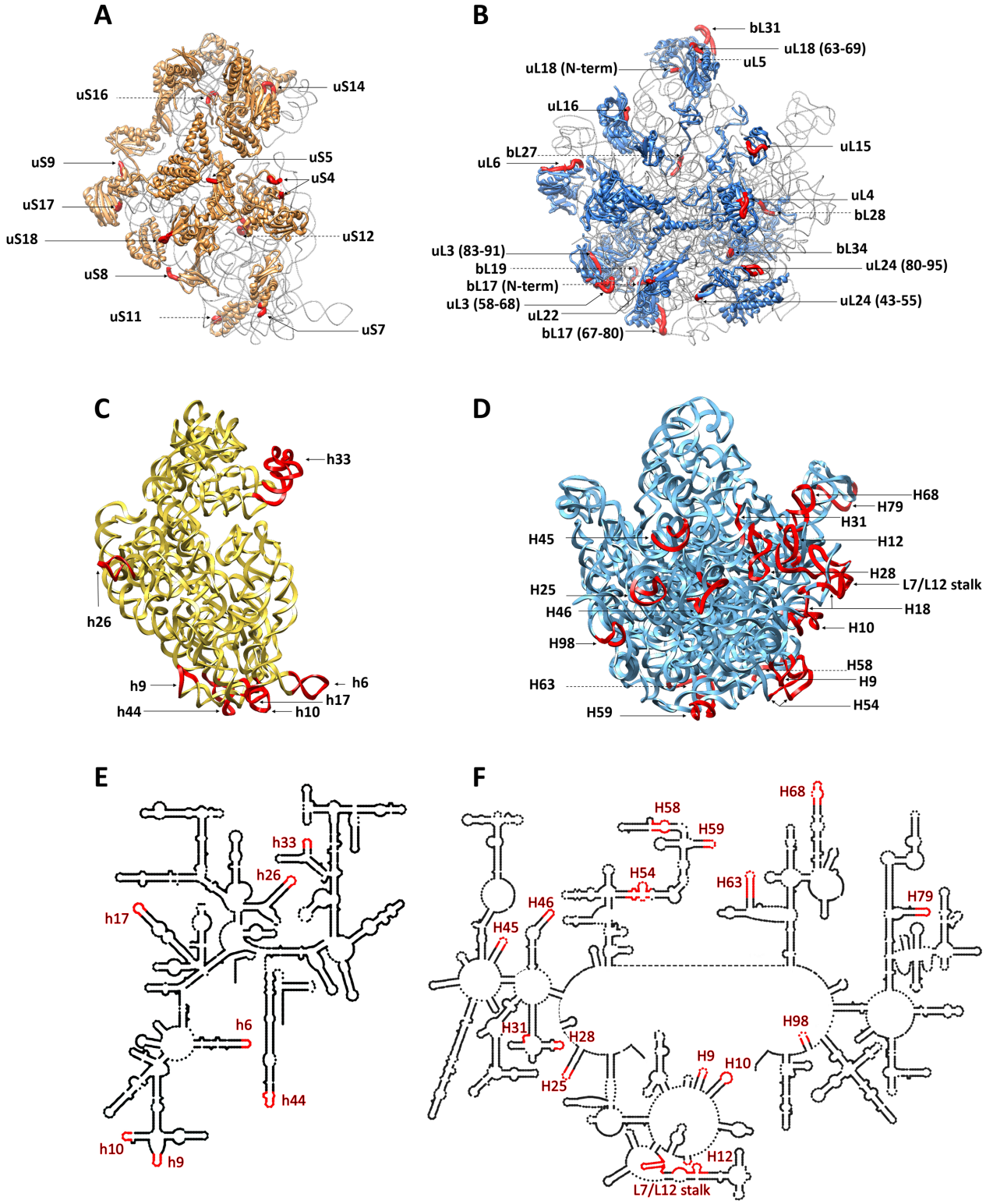

Figure 3. Structural differences at the RNA and the protein levels between representative bacterial species. (**A**) Cartoon rendering of ribosomal proteins from the SSU. In this and subsequent panels, the regions highlighted in red correspond to structural variability (insertions, deletions or alternative fold, shown in red) between the 70S ribosomes from *S. aureus, B. subtilis, E. coli* and *T. thermophilus*. (**B**) Same as (A) for the LSU. (**C**) Cartoon rendering of the three-dimensional structure of the 16S rRNA. (**D**) Same as (C) for the 5S and 23S rRNAs. (**E**) Secondary structure diagram of the model shown in (C). (**F**) Secondary structure diagram of the model shown in (D). A detailed description of all the differences between ribosomal proteins and RNAs are provided as Supplementary Tables S2 and S3.

Table 1. Data collection, refinement and validation statistics

Data collection	
Microscope	Titan Krios S-FEG
Camera	CMOS (Falcon II)
Volage (kV)	300
Magnification	59 000 X
Pixel size (Å.px^{-1})	1.1
Defocus range (μm)	(-4.5)–(-0.6)
Total dose (ē/Å^2)	60
Dose per frame	∼3.5
Micrographs collected	3872
Refinement	
Number of particles (total)	423 497
Number of particles (used for 3D reconstruction)	109 580
Resolution (Å; at FSC[a] = 0.143)	3.8
CC[a] (model to map fit[b])	0.76
Model composition	
Non-hydrogen atoms	140 840
Residues	10 185
Metal ions	32
RMS[a] deviations	
Bonds (Å)	0.011
Angles (°)	1.183
Chirality (°)	0.055
Planarity (°)	0.006
Validation[c]	
Clashscore[d]	4.49 (95th percentile)
Proteins	
MolProbity score	1.90 (81st percentile)
Favored rotamers	4536 (99.2%)
Ramachandran favored	4450 (84.9%)
Ramachandran allowed	778 (14.7%)
Ramachandran outliers	19 (0.4%)
RNA	
Correct sugar puckers	4571 (99.8%)
Correct backbone conformations	3664 (80.1%)

[a]FSC, Fourier shell correlation; CC, correlation coefficient; RMS, root-mean square
[b]Only across atoms in the model; compiled using Phenix (73)
[c]Compiled using MolProbity (80).
[d]Clashscore is the number of serious steric overlaps (>0.4 Å) per 1000 atoms.

(Figure 4A and B). The 15-amino-acid extension present in type B forms a loop that protrudes into the solvent, before the first beta strand. This observation led us to revise existing alignments of bL31 from Gram-positive and Gram-negative bacteria that placed the extension after the first or second Cys residues present in type A (27,41,43) (Figure 4C). Overall, this structure suggests that bL31 could accommodate large scale movements of the ribosome important for tRNA proofreading, similarly to type A that modulates the initial swivelling movements of the 30S subunit head domain (27).

At the rRNA level, several *S. aureus*-specific features can be found in our structure, some of which have already been described in the crystal structure of the LSU (51). For instance, the particular fold of H28 —a helix that interacts with uL4— is distinct from that in the other surveyed structures (Supplementary Figure S7C). Longer stems in *S. aureus* than in *T. thermophilus* are found in both the LSU (H10, H68) and the SSU (h6, h17, h26, h44) (Supplementary Table S3; Supplementary Figure S8; Figure 5A and B). Out of these various stem-loops protruding into the solvent, h26 is worth highlighting because of its interaction with the SD helix in the assembled translation initiation complex (84–87). The length of h26 is incremental when going from *T. thermophilus* (19 nt) through *E. coli* (25 nt) and *B. subtilis* (26 nt) to *S. aureus* (27 nt) which will affect its structure. Such variations at a strategical ribosomal region could be reflecting a species-specific involvement of h26 in translation initiation and regulation.

DISCUSSION

Exploring structural peculiarities in ribosomes is one of several complementary avenues toward understanding the mechanisms of translation and their regulation. A comparative analysis of our 3.8 Å cryo-EM structure of a 70S ribosome from *S. aureus* with other available structures of 70S ribosomes in various states demonstrates several examples of sites that could be involved in tuning translation in *S. aureus*. Notably, we observe that the presence or the absence of a structural element (protein or RNA) does not generally correspond to a particular group or division of bacteria. Exceptions to this principle require attention, as they may point to bacteria-specific mechanisms of translation regulation.

A striking example of ribosome diversity at the protein level is the bL31 protein, which is involved in controlling movements of the SSU with respect to the LSU during translation. Here, it is tempting to propose that the 15

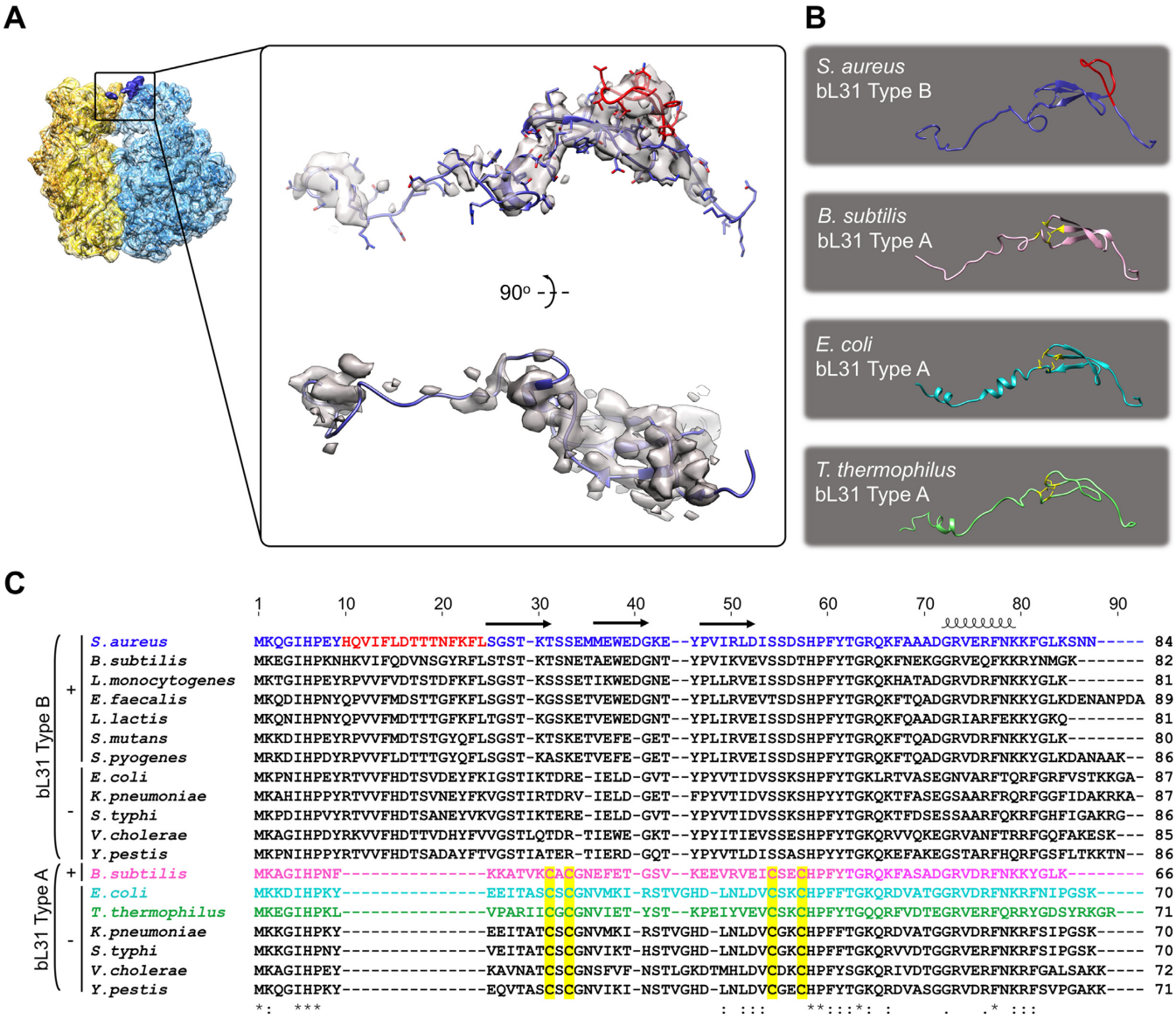

Figure 4. Structural homology of the bL31 type B protein bridge in absence of any Zinc-finger motif. (**A**) Protein bL31 forms an intersubunit bridge connecting the head of the 30S subunit with the central protuberance of the 50S subunit. The close up on the model of bL31 fitted into the cryo-EM density map reveals the localization of the extra loop (red) that is specific to non-zinc binding bL31 type B. (**B**) Comparison of the bL31 structures bound to the ribosome from four bacterial species: *S. aureus* (blue, this work); *B. subtilis* (pink, chain B3 in PDB ID 3J9W); *E. coli* (teal, chain 6 in PDB ID 5AFI); *T. thermophilus* (green, chain O in PDB ID 4W6F). Cysteine residues at the zinc-binding pocket in type A paralogs are shown in yellow. (**C**) Multiple sequence alignment of bL31 paralogs from representative Gram-positive (+) and Gram-negative (−) bacteria. Color-coding for sequences and Cys residues as in (B).

amino-acid extension specific to B-type paralogs impacts bL31's function. We already know that in *B. subtilis*, the B-type paralog of bL31 has a higher affinity for the ribosome than the A type (44). This property could be linked to folding adjustments that are made possible by the concomitant presence of the extension and absence of the Zn^{2+}-binding motif. Hence, B-type bL31 is likely to have altered dynamics on the ribosome in comparison with the A type, which would lead to better binding and modulation of subunit rotation. Additionally, another role for this loop could be to recruit regulatory factors. However, further studies are required in order for example to address whether the A-type bL31 confers particular properties to the ribosome under specific conditions, i.e. high intracellular concentrations of Zn^{2+}. The absence of A-type bL31 in *S. aureus* and many other Gram-positive pathogens (Figure 4C) remains intriguing as well, although it seems to be linked to the acquisition of alternative mechanisms for Zn^{2+} detoxification (88).

At the rRNA level, 7 helices on the SSU and 16 helices on the LSU were found to have different lengths or adopt different folds and orientations, as revealed when comparing the structures of 70S ribosomes from *E. coli*, *T. thermophilus* and *B. subtilis* (10,46–50,89) and the structure of the LSU from *S. aureus* (51) (Supplementary Figure S8). Many of them, such as h9, h26, h44 on the SSU and H9,

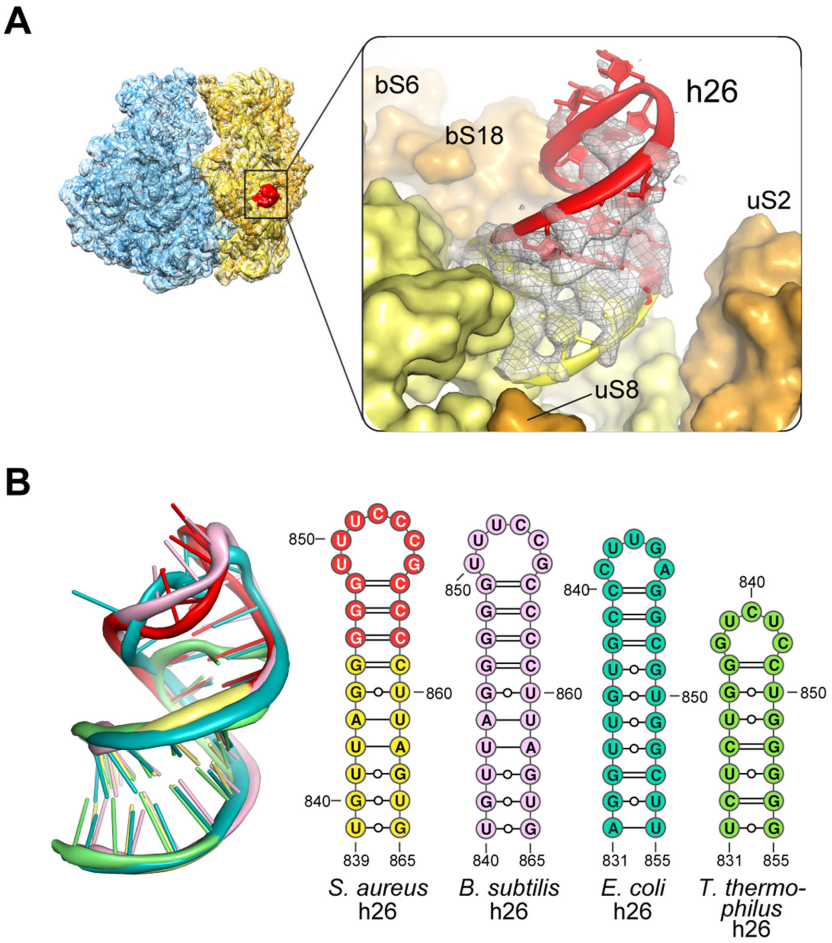

Figure 5. Helix h26 as a regulatory knob for translation? (**A**) Helix h26 protrudes from the surface of the SSU into the solvent (red, extension in *S. aureus* when compared to *T. thermophilus*; grey meshed surface, electron density; yellow surface, RNA; orange surface, proteins). (**B**) Superimposition of h26 from four bacteria (pink, *B. subtilis*, PDB ID 3J9W; teal, *E. coli,* PDB ID 4YBB; green, *T. thermophilus*, PDB ID 4V4J) with their corresponding 3D-based secondary structure.

H10, H25, H54, H63, H79, H98, are predominantly located on the solvent side of the ribosome. They also correspond to the expansion segments of eukaryotic ribosomes (6,7,58,90–92), which have been previously suggested to be involved in translation fine-tuning and ribosome biogenesis, potentially in a species-specific manner (91–93). Among these examples, h26 is a noteworthy one. Helix h26 is the insertion site for expansion segment 7 in eukaryotes, which is one of the largest in the SSU (from 15 nt in yeast and human to ∼140 nt in trypanosomatids), and is therefore thought to affect translation initiation in a major way by recruiting or preventing the recruitment of factors (20–22,91,92). In bacteria, h26 seems to be linked to a role in translation initiation and accommodation of the mRNA, through modulating interactions between the 16S rRNA (in particular at h23a, h26 and h45) and the mRNA, but also with proteins such as bS1, bS2, bS6, bS18 and bS21 (14,31,85,87,94). It is also possible that the U/C-rich apical loop of h26 in *S. aureus* (Figure 5B) would directly pair with the strong G-rich sequences found in many 5′ UTRs of *S. aureus* mRNAs, including the SD region (95–97), although this hypothesis remains to be tested. Nevertheless, these observations suggest that h26 might be involved in translation initiation regulation, in a species-specific manner.

Although our structure of the 70S ribosome from *S. aureus* reveals how some of the actors of ribosome heterogeneity like bL31 and h26 could be linked to translation regulation, it lacks information pertaining to bS1, bL9 (completely absent), bS21, uL1, bL7/bL12, uL10, uL11, part of bL25 (too flexible to be modeled). It suggests that their stabilization on the ribosome depends on ligands (mRNAs, tRNAs or translation factors). Ribosomal proteins such as bS1 and bL9 are hard to capture, because of their flexibility and their temporal association with the ribosome, which is linked to their requirement for translation of particular mRNAs, under certain environmental conditions (28,29,98). In the case of bL9, it would be interesting to study whether this protein is also involved in regulating translation slippage of particular mRNAs in *S. aureus*, as in for example *E. coli* upon their infection by T4 phages (98). Identifying such bL9-specific translation genes would enable us to adjust our growth and purification conditions so that bL9 would be incorporated into ribosome complexes prior to structural analysis. At that step, a closer monitoring of the transcrip-

tion levels of the bS1 and bL9 genes may be needed, in light of a recent transcriptomic study of *S. aureus*, which reported a decrease in the transcription of bS1 and bL9 genes upon addition of linezolid, suggesting a sensitive regulation of the synthesis of these two proteins (99). Studying polysomes of *S. aureus* ribosomes using cryo-electron tomography (100) could also reveal *S. aureus*-specific translation regulation mechanisms, in the case that bL9 would stabilize polysomes in *S. aureus* as it does in *E. coli* (101). Further cryo-EM analysis could also disclose the dynamic nature of the bL7/bL12 stalk, and whether its role in regulating the binding of translation factors is similar in *S. aureus* and in *E. coli* (102,103).

The absence of bS1 in our structure could further suggest that this protein is not required for anchoring mRNAs to the ribosome. As a further support to this hypothesis, we recently showed that ribosomes obtained from the same strain than the one used here (RN6390) and purified using the same procedure are able to form a ternary mRNA-tRNA-70S complex with *S. aureus* mRNAs carrying a short 5′ untranslated region and a strong SD sequence (104). In addition, as bS1 is devoid of its bS2-binding domain in *S. aureus*, it may no longer associate to the ribosome. It remains to be shown whether bS1 is in fact a typical ribosomal protein in *S. aureus*, or whether it acts outside the ribosome to modulate the translation of specific mRNAs.

Our structure provides an initial framework for understanding translation regulation in *S. aureus*. It hereby joins the pool of ribosome structures solved by X-ray crystallography (mostly for bacterial ribosomes) and cryo-EM (for both bacterial and eukaryotic ribosomes) that has been growing at a fast pace in recent years. Overall, a better characterization of translational aspects that occur under particular conditions or only in certain pathogenic species offers insights on novel strategies to combat infections. Remarkably, structures at (near)-atomic resolutions of ribosomes and other large macromolecular complexes bound to inhibitors are now within the reach of cryo-EM (7,105). Although the current resolution of our structure is on the low-end for exploring the structures of drug-ribosome complexes, it is close to that obtained for the LSU by X-ray crystallography (∼3.5 Å), and the continuous improvements in cryo-EM methodologies (1) are indicative that higher resolutions will be attainable within a short timeframe.

CONCLUSION

Having solved the structure of a vacant *S. aureus* ribosome at moderate resolution opens the door to determining the structures of ribosomes under physiological conditions and associated to trans-acting factors (translation factors, bS1, RNA helicases, etc.). Such structural studies would help unveil *S. aureus*-specific features of the translation machinery, so that we would better interpret how subtle structural differences impact the regulation of cellular metabolism and the cell's response to environmental changes. More generally, refining our understanding of translation regulation in *S. aureus* is another avenue toward exploring how RNA-dependent regulation in bacteria varies according to species-specific environmental and evolutionary constraints (106). Furthermore, a differential modulation of translation would potentially be synonymous with new drug targets, which would be of particular interest considering how multi-resistant *S. aureus* strains often are to conventional antibiotic treatments. Fine tuning our understanding of translation in *S. aureus* would thereby inform the design of antibiotics so that they would have lower effects on the human microbiome and would be less likely to elicit resistance. In this process, cryo-EM represents a powerful tool for solving ribosome complexes of pathogenic bacteria with antibiotics (105).

ACCESSION NUMBERS

Coordinates of the three-dimensional structure and cryo-EM map were deposited to the EMDB and PDB with accession numbers: EMDB ID: EMD-4050, PDB ID: 5LI0.

SUPPLEMENTARY DATA

Supplementary Data are available at NAR Online.

ACKNOWLEDGEMENTS

The authors wish to thank Pierre Fechter for his help in finding optimal conditions for cell lysis; Catherine Birck for her help with conducting analytical ultracentrifugation experiments; Philippe Hammann for managing the MS facility; Julien Moehlin for initial modeling and map fitting of the SSU; Francis Reyes and Simone Pellegrino for discussions regarding refinement at moderate resolution; Filip Leonarski, Luigi d'Ascenzo and Pascal Auffinger for their help with interpreting solvent binding sites; François Vandenesch for stimulating discussions; and Eric Westhof for ongoing support and helpful discussions.

FUNDING

'Centre National de la Recherche Scientifique' (CNRS) and the 'Agence Nationale de la Recherche' as part of the 'Investissements d'Avenir' program [LabEx: ANR-10-LABX-0036_NETRNA to P.R., Y.H.; ANR-15-CE11-0021-01 to G.Y.]; 'Fondation pour la Recherche Médicale en France' [FDT20140930867 to I.K.]. Funding for open access charge: Centre National de la Recherche Scientifique (CNRS).

Conflict of interest statement. None declared.

REFERENCES

1. Nogales,E. (2016) The development of cryo-EM into a mainstream structural biology technique. *Nat. Methods*, **13**, 24–27.
2. Eisenstein,M. (2016) The field that came in from the cold. *Nat. Methods*, **13**, 19–22.
3. Henderson,R. (2013) Avoiding the pitfalls of single particle cryo-electron microscopy: Einstein from noise. *Proc. Natl. Acad. Sci. U.S.A.*, **110**, 18037–18041.
4. des Georges,A., Dhote,V., Kuhn,L., Hellen,C.U., Pestova,T.V., Frank,J. and Hashem,Y. (2015) Structure of mammalian eIF3 in the context of the 43S preinitiation complex. *Nature*, **525**, 491–495.
5. Greber,B.J., Bieri,P., Leibundgut,M., Leitner,A., Aebersold,R., Boehringer,D. and Ban,N. (2015) Ribosome. The complete structure of the 55S mammalian mitochondrial ribosome. *Science*, **348**, 303–308.
6. Khatter,H., Myasnikov,A.G., Natchiar,S.K. and Klaholz,B.P. (2015) Structure of the human 80S ribosome. *Nature*, **520**, 640–645.

7. Wong,W., Bai,X.C., Brown,A., Fernandez,I.S., Hanssen,E., Condron,M., Tan,Y.H., Baum,J. and Scheres,S.H. (2014) Cryo-EM structure of the Plasmodium falciparum 80S ribosome bound to the anti-protozoan drug emetine. *Elife*, **3**, e03080.
8. Brown,A., Fernandez,I.S., Gordiyenko,Y. and Ramakrishnan,V. (2016) Ribosome-dependent activation of stringent control. *Nature*, **534**, 277–280.
9. Greber,B.J., Gerhardy,S., Leitner,A., Leibundgut,M., Salem,M., Boehringer,D., Leulliot,N., Aebersold,R., Panse,V.G. and Ban,N. (2016) Insertion of the biogenesis factor Rei1 probes the ribosomal tunnel during 60S maturation. *Cell*, **164**, 91–102.
10. Sohmen,D., Chiba,S., Shimokawa-Chiba,N., Innis,C.A., Berninghausen,O., Beckmann,R., Ito,K. and Wilson,D.N. (2015) Structure of the Bacillus subtilis 70S ribosome reveals the basis for species-specific stalling. *Nat. Commun.*, **6**, 6941.
11. Rotenberg,M.O., Moritz,M. and Woolford,J.L. Jr (1988) Depletion of Saccharomyces cerevisiae ribosomal protein L16 causes a decrease in 60S ribosomal subunits and formation of half-mer polyribosomes. *Genes Dev.*, **2**, 160–172.
12. Panina,E.M., Mironov,A.A. and Gelfand,M.S. (2003) Comparative genomics of bacterial zinc regulons: enhanced ion transport, pathogenesis, and rearrangement of ribosomal proteins. *Proc. Natl. Acad. Sci. U.S.A.*, **100**, 9912–9917.
13. Xue,S. and Barna,M. (2012) Specialized ribosomes: a new frontier in gene regulation and organismal biology. *Nat. Rev. Mol. Cell Biol.*, **13**, 355–369.
14. Byrgazov,K., Vesper,O. and Moll,I. (2013) Ribosome heterogeneity: Another level of complexity in bacterial translation regulation. *Curr. Opin. Microbiol.*, **16**, 133–139.
15. Yusupova,G. and Yusupov,M. (2014) High-resolution structure of the eukaryotic 80S ribosome. *Annu. Rev. Biochem.*, **83**, 467–486.
16. Komili,S., Farny,N.G., Roth,F.P. and Silver,P.A. (2007) Functional specificity among ribosomal proteins regulates gene expression. *Cell*, **131**, 557–571.
17. Yutin,N., Puigbo,P., Koonin,E.V. and Wolf,Y.I. (2012) Phylogenomics of prokaryotic ribosomal proteins. *PLoS One*, **7**, e36972.
18. Gunderson,J.H., Sogin,M.L., Wollett,G., Hollingdale,M., de la Cruz,V.F., Waters,A.P. and McCutchan,T.F. (1987) Structurally distinct, stage-specific ribosomes occur in Plasmodium. *Science*, **238**, 933–937.
19. Selker,E.U., Stevens,J.N. and Metzenberg,R.L. (1985) Heterogeneity of 5S RNA in fungal ribosomes. *Science*, **227**, 1340–1343.
20. Zwieb,C., Glotz,C. and Brimacombe,R. (1981) Secondary structure comparisons between small subunit ribosomal RNA molecules from six different species. *Nucleic Acids Res.*, **9**, 3621–3640.
21. Hassouna,N., Michot,B. and Bachellerie,J.P. (1984) The complete nucleotide sequence of mouse 28S rRNA gene. Implications for the process of size increase of the large subunit rRNA in higher eukaryotes. *Nucleic Acids Res.*, **12**, 3563–3583.
22. Ware,V.C., Tague,B.W., Clark,C.G., Gourse,R.L., Brand,R.C. and Gerbi,S.A. (1983) Sequence analysis of 28S ribosomal DNA from the amphibian Xenopus laevis. *Nucleic Acids Res.*, **11**, 7795–7817.
23. Gongadze,G.M., Korepanov,A.P., Korobeinikova,A.V. and Garber,M.B. (2008) Bacterial 5S rRNA-binding proteins of the CTC family. *Biochemistry (Mosc)*, **73**, 1405–1417.
24. Gongadze,G.M., Meshcheryakov,V.A., Serganov,A.A., Fomenkova,N.P., Mudrik,E.S., Jonsson,B.H., Liljas,A., Nikonov,S.V. and Garber,M.B. (1999) N-terminal domain, residues 1–91, of ribosomal protein TL5 from Thermus thermophilus binds specifically and strongly to the region of 5S rRNA containing loop E. *FEBS Lett.*, **451**, 51–55.
25. Lu,M. and Steitz,T.A. (2000) Structure of Escherichia coli ribosomal protein L25 complexed with a 5S rRNA fragment at 1.8-A resolution. *Proc. Natl. Acad. Sci. U.S.A.*, **97**, 2023–2028.
26. Stoldt,M., Wohnert,J., Ohlenschlager,O., Gorlach,M. and Brown,L.R. (1999) The NMR structure of the 5S rRNA E-domain-protein L25 complex shows preformed and induced recognition. *EMBO J.*, **18**, 6508–6521.
27. Jenner,L., Demeshkina,N., Yusupova,G. and Yusupov,M. (2010) Structural rearrangements of the ribosome at the tRNA proofreading step. *Nat. Struct. Mol. Biol.*, **17**, 1072–1078.
28. Duval,M., Korepanov,A., Fuchsbauer,O., Fechter,P., Haller,A., Fabbretti,A., Choulier,L., Micura,R., Klaholz,B.P., Romby,P. *et al.* (2013) Escherichia coli ribosomal protein S1 unfolds structured mRNAs onto the ribosome for active translation initiation. *PLoS Biol.*, **11**, e1001731.
29. Sorensen,M.A., Fricke,J. and Pedersen,S. (1998) Ribosomal protein S1 is required for translation of most, if not all, natural mRNAs in Escherichia coli in vivo. *J. Mol. Biol.*, **280**, 561–569.
30. Salah,P., Bisaglia,M., Aliprandi,P., Uzan,M., Sizun,C. and Bontems,F. (2009) Probing the relationship between Gram-negative and Gram-positive S1 proteins by sequence analysis. *Nucleic Acids Res.*, **37**, 5578–5588.
31. Byrgazov,K., Grishkovskaya,I., Arenz,S., Coudevylle,N., Temmel,H., Wilson,D.N., Djinovic-Carugo,K. and Moll,I. (2015) Structural basis for the interaction of protein S1 with the Escherichia coli ribosome. *Nucleic Acids Res.*, **43**, 661–673.
32. Diaconu,M., Kothe,U., Schlunzen,F., Fischer,N., Harms,J.M., Tonevitsky,A.G., Stark,H., Rodnina,M.V. and Wahl,M.C. (2005) Structural basis for the function of the ribosomal L7/12 stalk in factor binding and GTPase activation. *Cell*, **121**, 991–1004.
33. McGinness,K.E. and Sauer,R.T. (2004) Ribosomal protein S1 binds mRNA and tmRNA similarly but plays distinct roles in translation of these molecules. *Proc. Natl. Acad. Sci. U.S.A.*, **101**, 13454–13459.
34. van Duin,J. and van Knippenberg,P.H. (1974) Functional heterogeneity of the 30 S ribosomal subunit of Escherichia coli. 3. Requirement of protein S1 for translation. *J. Mol. Biol.*, **84**, 185–195.
35. van Knippenberg,P.H., Hooykaas,P.J. and van Duin,J. (1974) The stoichiometry of E. coli 30S ribosomal protein S1 on in vivo and in vitro polyribosomes. *FEBS Lett.*, **41**, 323–326.
36. Kaberdina,A.C., Szaflarski,W., Nierhaus,K.H. and Moll,I. (2009) An unexpected type of ribosomes induced by kasugamycin: a look into ancestral times of protein synthesis? *Mol. Cell*, **33**, 227–236.
37. Vesper,O., Amitai,S., Belitsky,M., Byrgazov,K., Kaberdina,A.C., Engelberg-Kulka,H. and Moll,I. (2011) Selective translation of leaderless mRNAs by specialized ribosomes generated by MazF in Escherichia coli. *Cell*, **147**, 147–157.
38. Schmalisch,M., Langbein,I. and Stulke,J. (2002) The general stress protein Ctc of Bacillus subtilis is a ribosomal protein. *J. Mol. Microbiol. Biotechnol.*, **4**, 495–501.
39. Völker,U., Engelmann,S., Maul,B., Riethdorf,S., Völker,A., Schmid,R., Mach,H. and Hecker,M. (1994) Analysis of the induction of general stress proteins of *Bacillus subtilis*. *Microbiology*, **140**, 741–752.
40. Gordiyenko,Y., Deroo,S., Zhou,M., Videler,H. and Robinson,C.V. (2008) Acetylation of L12 increases interactions in the Escherichia coli ribosomal stalk complex. *J. Mol. Biol.*, **380**, 404–414.
41. Makarova,K.S., Ponomarev,V.A. and Koonin,E.V. (2001) Two C or not two C: Recurrent disruption of Zn-ribbons, gene duplication, lineage-specific gene loss, and horizontal gene transfer in evolution of bacterial ribosomal proteins. *Genome Biol.*, **2**, RESEARCH 0033.
42. Gaballa,A. and Helmann,J.D. (1998) Identification of a zinc-specific metalloregulatory protein, Zur, controlling zinc transport operons in Bacillus subtilis. *J. Bacteriol.*, **180**, 5815–5821.
43. Nanamiya,H., Akanuma,G., Natori,Y., Murayama,R., Kosono,S., Kudo,T., Kobayashi,K., Ogasawara,N., Park,S.M., Ochi,K. *et al.* (2004) Zinc is a key factor in controlling alternation of two types of L31 protein in the Bacillus subtilis ribosome. *Mol. Microbiol.*, **52**, 273–283.
44. Akanuma,G., Nanamiya,H., Natori,Y., Nomura,N. and Kawamura,F. (2006) Liberation of zinc-containing L31 (RpmE) from ribosomes by its paralogous gene product, YtiA, in Bacillus subtilis. *J. Bacteriol.*, **188**, 2715–2720.
45. Wall,E.A., Caufield,J.H., Lyons,C.E., Manning,K.A., Dokland,T. and Christie,G.E. (2015) Specific N-terminal cleavage of ribosomal protein L27 in Staphylococcus aureus and related bacteria. *Mol. Microbiol.*, **95**, 258–269.
46. Schuwirth,B.S., Borovinskaya,M.A., Hau,C.W., Zhang,W., Vila-Sanjurjo,A., Holton,J.M. and Cate,J.H. (2005) Structures of the bacterial ribosome at 3.5 A resolution. *Science*, **310**, 827–834.
47. Noeske,J., Wasserman,M.R., Terry,D.S., Altman,R.B., Blanchard,S.C. and Cate,J.H. (2015) High-resolution structure of the Escherichia coli ribosome. *Nat. Struct. Mol. Biol.*, **22**, 336–341.
48. Yusupov,M.M., Yusupova,G.Z., Baucom,a., Lieberman,K., Earnest,T.N., Cate,J.H. and Noller,H.F. (2001) Crystal structure of the ribosome at 5.5 A resolution. *Science*, **292**, 883–896.

49. Yusupova,G., Jenner,L., Rees,B., Moras,D. and Yusupov,M. (2006) Structural basis for messenger RNA movement on the ribosome. *Nature*, **444**, 391–394.
50. Selmer,M., Dunham,C.M., Murphy,F.V.t., Weixlbaumer,A., Petry,S., Kelley,A.C., Weir,J.R. and Ramakrishnan,V. (2006) Structure of the 70S ribosome complexed with mRNA and tRNA. *Science*, **313**, 1935–1942.
51. Eyal,Z., Matzov,D., Krupkin,M., Wekselman,I., Paukner,S., Zimmerman,E., Rozenberg,H., Bashan,A. and Yonath,A. (2015) Structural insights into species-specific features of the ribosome from the pathogen Staphylococcus aureus. *Proc. Natl. Acad. Sci. U.S.A.*, **112**, E5805–E5814.
52. Yusupova,G. and Yusupov,M. (2015) Ribosome biochemistry in crystal structure determination. *RNA*, **21**, 771–773.
53. Harms,J., Schluenzen,F., Zarivach,R., Bashan,A., Gat,S., Agmon,I., Bartels,H., Franceschi,F. and Yonath,A. (2001) High resolution structure of the large ribosomal subunit from a mesophilic eubacterium. *Cell*, **107**, 679–688.
54. Grice,E.A. and Segre,J.A. (2011) The skin microbiome. *Nat. Rev. Microbiol.*, **9**, 244–253.
55. Powers,M.E. and Bubeck Wardenburg,J. (2014) Igniting the fire: Staphylococcus aureus virulence factors in the pathogenesis of sepsis. *PLoS Pathog.*, **10**, e1003871.
56. Zecconi,A. and Scali,F. (2013) Staphylococcus aureus virulence factors in evasion from innate immune defenses in human and animal diseases. *Immunol. Lett.*, **150**, 12–22.
57. Beenken,K.E., Blevins,J.S. and Smeltzer,M.S. (2003) Mutation of sarA in Staphylococcus aureus limits biofilm formation. *Infect. Immun.*, **71**, 4206–4211.
58. Ben-Shem,A., Garreau de Loubresse,N., Melnikov,S., Jenner,L., Yusupova,G. and Yusupov,M. (2011) The structure of the eukaryotic ribosome at 3.0 Å resolution. *Science*, **334**, 1524–1529.
59. Schuck,P. (2000) Size-distribution analysis of macromolecules by sedimentation velocity ultracentrifugation and lamm equation modeling. *Biophys. J.*, **78**, 1606–1619.
60. de la Rosa-Trevin,J.M., Quintana,A., Del Cano,L., Zaldivar,A., Foche,I., Gutierrez,J., Gomez-Blanco,J., Burguet-Castell,J., Cuenca-Alba,J., Abrishami,V. *et al.* (2016) Scipion: A software framework toward integration, reproducibility and validation in 3D electron microscopy. *J. Struct. Biol.*, **195**, 93–99.
61. de la Rosa-Trevin,J.M., Oton,J., Marabini,R., Zaldivar,A., Vargas,J., Carazo,J.M. and Sorzano,C.O. (2013) Xmipp 3.0: An improved software suite for image processing in electron microscopy. *J. Struct. Biol.*, **184**, 321–328.
62. Rohou,A. and Grigorieff,N. (2015) CTFFIND4: Fast and accurate defocus estimation from electron micrographs. *J. Struct. Biol.*, **192**, 216–221.
63. Abrishami,V., Zaldivar-Peraza,A., de la Rosa-Trevin,J.M., Vargas,J., Oton,J., Marabini,R., Shkolnisky,Y., Carazo,J.M. and Sorzano,C.O. (2013) A pattern matching approach to the automatic selection of particles from low-contrast electron micrographs. *Bioinformatics*, **29**, 2460–2468.
64. Scheres,S.H. (2012) RELION: implementation of a Bayesian approach to cryo-EM structure determination. *J. Struct. Biol.*, **180**, 519–530.
65. Kucukelbir,A., Sigworth,F.J. and Tagare,H.D. (2014) Quantifying the local resolution of cryo-EM density maps. *Nat. Methods*, **11**, 63–65.
66. Pettersen,E.F., Goddard,T.D., Huang,C.C., Couch,G.S., Greenblatt,D.M., Meng,E.C. and Ferrin,T.E. (2004) UCSF Chimera–a visualization system for exploratory research and analysis. *J. Comput. Chem.*, **25**, 1605–1612.
67. Jossinet,F., Ludwig,T.E. and Westhof,E. (2010) Assemble: an interactive graphical tool to analyze and build RNA architectures at the 2D and 3D levels. *Bioinformatics*, **26**, 2057–2059.
68. Biasini,M., Bienert,S., Waterhouse,A., Arnold,K., Studer,G., Schmidt,T., Kiefer,F., Gallo Cassarino,T., Bertoni,M., Bordoli,L. *et al.* (2014) SWISS-MODEL: Modelling protein tertiary and quaternary structure using evolutionary information. *Nucleic Acids Res.*, **42**, W252–W258.
69. Trabuco,L.G., Villa,E., Mitra,K., Frank,J. and Schulten,K. (2008) Flexible fitting of atomic structures into electron microscopy maps using molecular dynamics. *Structure*, **16**, 673–683.
70. Humphrey,W., Dalke,A. and Schulten,K. (1996) VMD: visual molecular dynamics. *J. Mol. Graph.*, **14**, 27–38.
71. Phillips,J.C., Braun,R., Wang,W., Gumbart,J., Tajkhorshid,E., Villa,E., Chipot,C., Skeel,R.D., Kale,L. and Schulten,K. (2005) Scalable molecular dynamics with NAMD. *J. Comput. Chem.*, **26**, 1781–1802.
72. Adams,P.D., Afonine,P.V., Bunkoczi,G., Chen,V.B., Davis,I.W., Echols,N., Headd,J.J., Hung,L.W., Kapral,G.J., Grosse-Kunstleve,R.W. *et al.* (2010) PHENIX: A comprehensive Python-based system for macromolecular structure solution. *Acta Crystallogr. D Biol. Crystallogr.*, **66**, 213–221.
73. Afonine,P., Headd,J., Terwilliger,T. and Adams,P. (2013) New tool: phenix. real_space_refine. *Comput. Crystallogr. Newsl.*, **4**, 43–44.
74. Chou,F.C., Sripakdeevong,P., Dibrov,S.M., Hermann,T. and Das,R. (2013) Correcting pervasive errors in RNA crystallography through enumerative structure prediction. *Nat. Methods*, **10**, 74–76.
75. Jain,S., Richardson,D.C. and Richardson,J.S. (2015) Computational methods for RNA structure validation and improvement. *Methods Enzymol.*, **558**, 181–212.
76. Emsley,P. and Cowtan,K. (2004) Coot: Model-building tools for molecular graphics. *Acta Crystallogr. D Biol. Crystallogr.*, **60**, 2126–2132.
77. Keating,K.S. and Pyle,A.M. (2012) RCrane: semi-automated RNA model building. *Acta Crystallogr. D Biol. Crystallogr.*, **68**, 985–995.
78. Leonarski,F., D'Ascenzo,L. and Auffinger,P. (2016) Binding of metals to purine N7 nitrogen atoms and implications for nucleic acids: A CSD survey. *Inorganica Chim. Acta*, **452**, 82–89.
79. Martinez,J.M., Pappalardo,R.R. and Marcos,E.S. (1999) Shape and size of simple cations in aqueous solutions: A theoretical reexamination of the hydrated ion via computer simulations. *J. Chem. Phys.*, **110**, 1669–1676.
80. Chen,V.B., Arendall,W.B. 3rd, Headd,J.J., Keedy,D.A., Immormino,R.M., Kapral,G.J., Murray,L.W., Richardson,J.S. and Richardson,D.C. (2010) MolProbity: All-atom structure validation for macromolecular crystallography. *Acta Crystallogr. D Biol. Crystallogr.*, **66**, 12–21.
81. Gogiya,Z.V., Yusupov,M.M. and Spirina,T.N. (1986) Structure of Thermus-Thermophilus ribosomes .1. Method for isolation and purification of ribosomes. *Mol. Biol.*, **20**, 415–421.
82. Fechter,P., Chevalier,C., Yusupova,G., Yusupov,M., Romby,P. and Marzi,S. (2009) Ribosomal initiation complexes probed by toeprinting and effect of trans-acting translational regulators in bacteria. *Methods Mol. Biol.*, **540**, 247–263.
83. Rozov,A., Demeshkina,N., Westhof,E., Yusupov,M. and Yusupova,G. (2015) Structural insights into the translational infidelity mechanism. *Nat. Commun.*, **6**, 7251.
84. Gualerzi,C.O. and Pon,C.L. (2015) Initiation of mRNA translation in bacteria: structural and dynamic aspects. *Cell Mol. Life Sci.*, **72**, 4341–4367.
85. Korostelev,A., Trakhanov,S., Asahara,H., Laurberg,M., Lancaster,L. and Noller,H.F. (2007) Interactions and dynamics of the Shine Dalgarno helix in the 70S ribosome. *Proc. Natl. Acad. Sci. U.S.A.*, **104**, 16840–16843.
86. Kaminishi,T., Wilson,D.N., Takemoto,C., Harms,J.M., Kawazoe,M., Schluenzen,F., Hanawa-Suetsugu,K., Shirouzu,M., Fucini,P. and Yokoyama,S. (2007) A snapshot of the 30S ribosomal subunit capturing mRNA via the Shine-Dalgarno interaction. *Structure*, **15**, 289–297.
87. Marzi,S., Myasnikov,A.G., Serganov,A., Ehresmann,C., Romby,P., Yusupov,M. and Klaholz,B.P. (2007) Structured mRNAs regulate translation initiation by binding to the platform of the ribosome. *Cell*, **130**, 1019–1031.
88. Singh,V.K., Xiong,A., Usgaard,T.R., Chakrabarti,S., Deora,R., Misra,T.K. and Jayaswal,R.K. (1999) ZntR is an autoregulatory protein and negatively regulates the chromosomal zinc resistance operon znt of Staphylococcus aureus. *Mol. Microbiol.*, **33**, 200–207.
89. Rozov,A., Westhof,E., Yusupov,M. and Yusupova,G. (2016) The ribosome prohibits the G.U wobble geometry at the first position of the codon-anticodon helix. *Nucleic Acids Res.*, **44**, 6434–6441.
90. Anger,A.M., Armache,J.P., Berninghausen,O., Habeck,M., Subklewe,M., Wilson,D.N. and Beckmann,R. (2013) Structures of the human and Drosophila 80S ribosome. *Nature*, **497**, 80–85.

91. Gao,H., Ayub,M.J., Levin,M.J. and Frank,J. (2005) The structure of the 80S ribosome from Trypanosoma cruzi reveals unique rRNA components. *Proc. Natl. Acad. Sci. U.S.A.*, **102**, 10206–10211.
92. Hashem,Y., des Georges,A., Fu,J., Buss,S.N., Jossinet,F., Jobe,A., Zhang,Q., Liao,H.Y., Grassucci,R.A., Bajaj,C. *et al.* (2013) High-resolution cryo-electron microscopy structure of the Trypanosoma brucei ribosome. *Nature*, **494**, 385–389.
93. Ramesh,M. and Woolford,J.L. Jr (2016) Eukaryote-specific rRNA expansion segments function in ribosome biogenesis. *RNA*, **22**, 1153–1162.
94. Sengupta,J., Agrawal,R.K. and Frank,J. (2001) Visualization of protein S1 within the 30S ribosomal subunit and its interaction with messenger RNA. *Proc. Natl. Acad. Sci. U.S.A.*, **98**, 11991–11996.
95. Boisset,S., Geissmann,T., Huntzinger,E., Fechter,P., Bendridi,N., Possedko,M., Chevalier,C., Helfer,A.C., Benito,Y., Jacquier,A. *et al.* (2007) Staphylococcus aureus RNAIII coordinately represses the synthesis of virulence factors and the transcription regulator Rot by an antisense mechanism. *Genes Dev.*, **21**, 1353–1366.
96. Huntzinger,E., Boisset,S., Saveanu,C., Benito,Y., Geissmann,T., Namane,A., Lina,G., Etienne,J., Ehresmann,B., Ehresmann,C. *et al.* (2005) Staphylococcus aureus RNAIII and the endoribonuclease III coordinately regulate spa gene expression. *EMBO J.*, **24**, 824–835.
97. Chang,B., Halgamuge,S. and Tang,S.L. (2006) Analysis of SD sequences in completed microbial genomes: non-SD-led genes are as common as SD-led genes. *Gene*, **373**, 90–99.
98. Wilson,D.N. and Nierhaus,K.H. (2005) Ribosomal proteins in the spotlight. *Crit. Rev. Biochem. Mol. Biol.*, **40**, 243–267.
99. Bonn,F., Pane-Farre,J., Schluter,R., Schaffer,M., Fuchs,S., Bernhardt,J., Riedel,K., Otto,A., Volker,U., van Dijl,J.M. *et al.* (2016) Global analysis of the impact of linezolid onto virulence factor production in S. aureus USA300. *Int. J. Med. Microbiol.*, **306**, 131–140.
100. Brandt,F., Carlson,L.A., Hartl,F.U., Baumeister,W. and Grunewald,K. (2010) The three-dimensional organization of polyribosomes in intact human cells. *Mol. Cell*, **39**, 560–569.
101. Dunkle,J. and Cate,J.H.D. (2011) In: Rodnina,MV, Wintermeyer,W and Green,R (eds). *Ribosomes - Structure, Function, and Dynamics*. Springer, pp. 65–73.
102. Agrawal,R.K., Lata,R.K. and Frank,J. (1999) Conformational variability in Escherichia coli 70S ribosome as revealed by 3D cryo-electron microscopy. *Int. J. Biochem. Cell Biol.*, **31**, 243–254.
103. Agrawal,R.K., Penczek,P., Grassucci,R.A. and Frank,J. (1998) Visualization of elongation factor G on the Escherichia coli 70S ribosome: the mechanism of translocation. *Proc. Natl. Acad. Sci. U.S.A.*, **95**, 6134–6138.
104. Khusainov,I., Marenna,A., Cerciat,M., Fechter,P., Hashem,Y., Marzi,S., Romby,P., Yusupova,G. and Yusupov,M. (2016) A glimpse on *Staphylococcus aureus* translation machinery and its control. *Mol. Biol. (Mosk)*, **50**, 549–557.
105. Merk,A., Bartesaghi,A., Banerjee,S., Falconieri,V., Rao,P., Davis,M.I., Pragani,R., Boxer,M.B., Earl,L.A., Milne,J.L. *et al.* (2016) Breaking Cryo-EM resolution barriers to facilitate drug discovery. *Cell*, **165**, 1698–1707.
106. Felden,B., Vandenesch,F., Bouloc,P. and Romby,P. (2011) The Staphylococcus aureus RNome and its commitment to virulence. *PLoS Pathog.*, **7**, e1002006.